DOI: 10.1002/ejic.201100536

One-Pot Synthesis of Core-Shell Silver-Gold Nanoparticle Solutions and Their Interaction with Methylene Blue Dye

Madeeha A. Uppal,[a] Michael B. Ewing,[a] and Ivan P. Parkin*[a]

Keywords: Nanoparticles / Colloids / Silver / Gold / Dyes / Metal–Dye interactions

A one-pot modified Turkevich synthesis was used to synthesise a range of colloids from pure Ag, through Ag/Au core-shell mixtures to pure Au by the thermal co-addition of trisodium citrate to auric acid and silver nitrate mixtures. The colloids were analysed by means of XRD and wide-beam energy dispersive X-ray (EDX) analysis. The UV/Vis spectroscopy showed a non-linear variation in the surface plasmon resonance band with the Au/Ag ratio, consistent with core-shell formation. High resolution transmission electron microscopy (HRTEM) imaging, in conjunction with thin-beam EDX line analysis, confirmed the presence of predominantly Ag cores and Au exteriors in the Au/Ag mixture. The argon ion sputtering with X-ray photoelectron spectroscopy (XPS) measurements of the particles also indicated a Ag-Au core-shell formation. Ag^0, Au^0 and significant levels of Au^I states were observed, which correlate with a Ag-Au core-shell model where the gold shell becomes partially oxidised at the surface. The subsequent titration of the colloids with methylene blue (MB) dye showed strong positive increases in the extinction coefficient at the absorption maximum. At the optimum levels of dye addition, a linear relationship was found between the average nanoparticle size and the number of dye solvation shells. The pure Au and Ag colloids showed the greatest propensity for an increase in the extinction coefficient of MB due to an enhanced transfer of the surface plasmons to the localised dye molecules and demonstrated the potential for increased functionality as light-activated agents in the lethal photosensitisation of bacteria.

Introduction

Recently, much attention has been paid to the synthesis and characterisation of bimetallic nanoparticles due to their unique catalytic, electronic, optical, structural and thermal properties[1–4] and the subsequent technological applications of these nanoparticles as catalysts, sensors, nano-electronic devices[5–12] and biosensors.[13] It is currently understood that the versatility of these nano-materials may be attributed to their size and shape-dependent properties,[12] however, the combination of the component metals and their fine structure, either as an alloy or a core-shell structure, are tuneable factors that also contribute to the bimetallic systems.[14–16] The five different bimetallic nanoparticle formulations that can form for gold and silver are shown in Scheme 1. Investigations into bimetallic noble metal alloy combinations such as Pt-Ru, Cu-Pd, Pt-Mo, Pt-W, Pt-Ni and Au-Ag have been made,[17–21] where the Au-Ag combination is the most extensively studied due, in part, to the fact that both the Ag and Au nanoparticles display distinctive optical plasmon absorbances in the visible range.[22–25] The optical and catalytic properties of the Ag and Au nanoparticles are useful in a diverse range of applications.

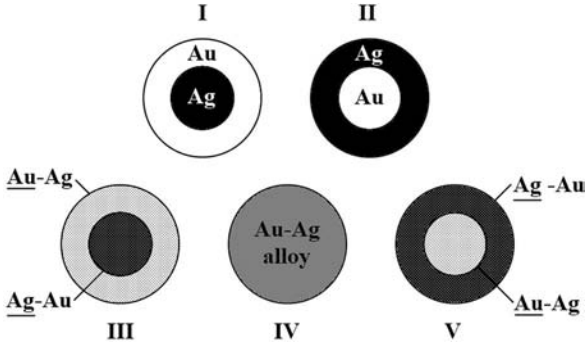

Scheme 1. A diagram displaying the five different types of bimetallic nanoparticles that can form when the gold and silver constituents are combined. Type I = Ag core – Au shell, type II = Au core – Ag shell, type III = Ag rich core – Au rich shell, type IV = pure Au – Ag alloy, type V = Au rich core – Ag rich shell.

Current research has employed Au and Ag nanoparticles for the enhancement of the optical properties in semiconductor thin films by means of composite formation,[26–33] the destruction of bacteria,[34–40] photo switches,[41] improvements in the detection of cancer[42] and DNA,[43] and even for single molecule detection by means of surface enhanced Raman spectroscopy (SERS).[44,45] By combining these two metals into a single entity, the catalytic properties can be further enhanced[11] and the localised surface plasmon absorption can be varied continuously between the limits of the monometallic Au and Ag nanoparticles.[24]

[a] Department of Chemistry, University College London, 20 Gordon Street, London, WC1H 0AJ, United Kingdom
Fax: +44-20-7679-7463
E-mail: i.p.parkin@ucl.ac.uk

Overall, Ag and Au form alloys for all of the compositions with very little surface segregation due to their analogous face-centred cubic packing with the almost identical lattice constants of 4.086 Å and 4.073 Å, respectively, and with very similar chemical properties.[46,47] Nanoparticles with either the alloyed (Scheme 1, Type IV)[48–65] or the core–shell segregated structure (Scheme 1, Types I and II) can be synthesised through various methods.[66–68] The most common formation of a Au-Ag alloy uses a Turkevich-type co-reduction of the metal precursors in the presence of a stabilising agent, such as trisodium citrate in water or microemulsion.[48–55] The other routes include inverse micelle,[56] replacement reactions,[57,58] laser-assisted,[59,60] alcohol reduction,[61] borohydride reduction,[62] laser ablation,[63] ultrasound irradiation[64] and metal evaporation-condensation methods.[65] However, the core-shell Ag-Au colloid formations that have been reported in the literature are dominated by the two-step seed-mediated growth process.[66–68]

Dyes that were deposited onto the Au and Ag surfaces have shown an increase in their light absorption. This is due to an excitation transfer from the metallic surface to the absorbed dye.[69] Similarly, the Au, Ag and Au-Ag alloy colloidal nanoparticles show this phenomenon.[70–72] The absorption of methylene blue dye onto gold has shown applications that are of particular interest for the formation of antimicrobial polymers[40] and polymer substrates for SERS.[73] Methylene blue (MB) dye was recently established as a light-activated agent in the lethal photosensitisation of bacteria.[87,88] The light absorbed by the dye generates excited triplet states that interact with oxygen to generate singlet oxygen. Singlet oxygen is highly reactive and can damage cell walls, plasma membranes and DNA, which leads to microbial cell death. By enhancing the level of light that MB can absorb, through its absorption and interaction with the nanoparticle colloids, it is quite feasible that greater levels of singlet oxygen may be produced when it is employed as a light-activated antibacterial agent. The optical and scattering properties of the Au-Ag colloids have been investigated by monitoring the effect of methylene blue and anionic cyanine dye absorption on the alloy.[70,74] However, to the best of our knowledge, the enhancement of the extinction coefficient of the dyes upon the Ag-Au core-shell nanoparticles has not been reported to date.

Herein we present a new reduction method for the one-step production of core-shell Ag-Au nanoparticles, which consist primarily of a Ag core and a Au outer-shell that was synthesised by means of a modified Turkevich approach (Scheme 1, Type III). The near monodispersity of the aggregates was accomplished by the induction of digestive ripening by continued reflux. The aggregates, which had a varying Au/Ag ratio, were characterised by using UV/Vis spectroscopy, energy dispersive X-ray (EDX) analysis, XRD, high resolution transmission electron microscopy (HRTEM), which was equipped with a thin-beam EDX probe, and X-ray photoelectron spectroscopy (XPS) with argon sputtering. The excitation transfer from these core-shell nanoparticles, compared with both the pure Ag and Au nanoparticles, to the methylene blue dye molecules was probed with UV/Vis spectroscopy. It was noted that the extinction coefficient of methylene blue was significantly enhanced by its absorption onto the nanoparticle and that either pure Ag or pure Au nanoparticles gave the greatest enhancement. To the best of our knowledge, this is the first reported case of the synthesis of core-shell Ag-Au nanoparticles by means of a single step and without the use of seeding procedures. The formation of the core-shell particles in this synthesis shed light on the reaction mechanism and showed that silver nitrate reacts faster than auric acid in the Turkevich process under these conditions.

Results and Discussion

The gold, silver and gold-silver colloidal suspensions were prepared by the co-addition of the sodium citrate solution to the heated auric acid and silver nitrate mixture with the predetermined Au/Ag ratios, which were 100% Au, 75% Au: 25% Ag, 50% Au: 50% Ag, 25% Au: 75% Ag and 100% Ag. The solutions were heated under reflux in order to encourage monodispersity through digestive ripening.[74] The solutions were topped up to 40 mL with distilled water in order to form colloids with an equivalent metal content (2.5 μM). The solution colours ranged from pale yellow (pure Ag) to pink/red (pure Au) with intermediate hues for the varying metal combinations as shown in Figure 1.

Figure 1. The Au, Ag and Au/Ag core-shell (Ag core-Au shell) colloidal suspensions were prepared by a modified Turkevich thermal co-addition of the sodium citrate solution to the auric acid and silver nitrate mixtures with the predetermined Au/Ag ratios of 100% Au, 75% Au: 25%Ag, 50% Au: 50% Ag, 25% Au: 75% Ag and 100% Ag. The solutions are displayed in the image above from the greatest silver content on the left (Ag 100%) to the greatest gold content on the right (Au 100%).

The spectroscopic profiles of the nanoparticle colloids were assessed with UV/Vis spectroscopy. A stacked plot of the spectra normalised to the heights of their respective SPR band centres is displayed in Figure 2 (a). A general trend of an increasing SPR wavelength centre was observed on going from pure Ag to pure Au. However, slight side bands were observed at approximately 320 nm in both the 25% Au: 75% Ag and the 100% Ag samples, which indicated a non-transitional range of nanoparticle sizes. The wide SPR bands that are seen in the 75% Au: 25% Ag and 50% Au: 50% samples indicated that a comparatively broader range of particle sizes formed and were, most probably, more polydisperse. In addition, each of the solutions showed a single SPR band, which indicated that the solutions did not consist of pure Au and Ag nanoparticle mixtures, which would show individual SPR bands at approximately 385 and 520 nm for Ag and Au, respectively. Where

Au-Ag bimetallic nanoparticles form alloys, a linear relationship between the surface plasmon resonance centre and the Au/Ag metal content is observed.[53] However, a non-linear relationship between these plasmon resonance centres and the Ag metal composition was observed in this study, as shown in Figure 2 (b). This indicated the formation of core-shell type nanoparticles as predicted by the Mie theory[54] and it fits a Boltzmann model with good agreement (r^2 = 0.98). The slight blue-shift in the SPR centre of the 25% Au: 75% Ag sample compared to that of pure silver was attributed to significant differences in the average nanoparticle diameter.[74] Although the metal concentrations were equivalent, the SPR absorbance of the pure Ag nanoparticles was far greater than that of the pure Au, and a steady decrease in the absorbance for the core-shell Au/Ag colloids was observed with the increase in the Au content. The XRD patterns of the colloids formed in this study had primitive face-centred cubic (FCC) symmetry, which is analogous to their bulk gold ($FM\bar{3}M$, a = 4.083 Å) and silver ($FM\bar{3}M$, a = 4.068 Å) counterparts. A stacked plot of the corresponding diffraction patterns is displayed in Figure 3.

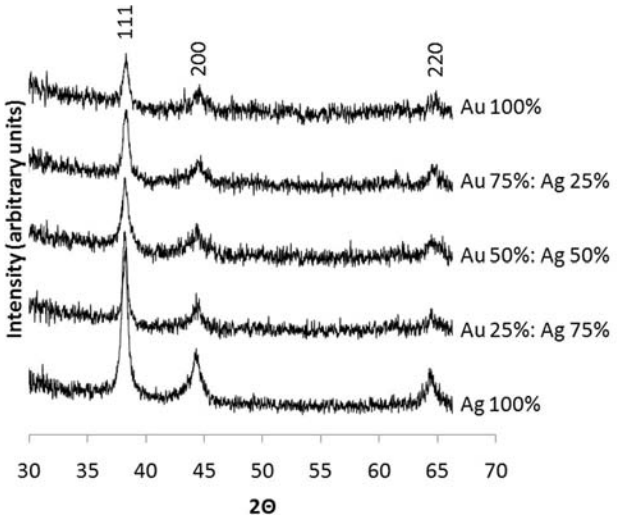

Figure 3. A stacked plot of the XRD diffraction patterns that were acquired for the Au, Ag and Au/Ag core-shell (Ag core-Au shell) colloidal suspensions that were deposited on silica. The nanoparticles were synthesised by a modified Turkevich thermal co-addition of trisodium citrate to the auric acid and silver nitrate mixtures with a predetermined Au/Ag ratio.

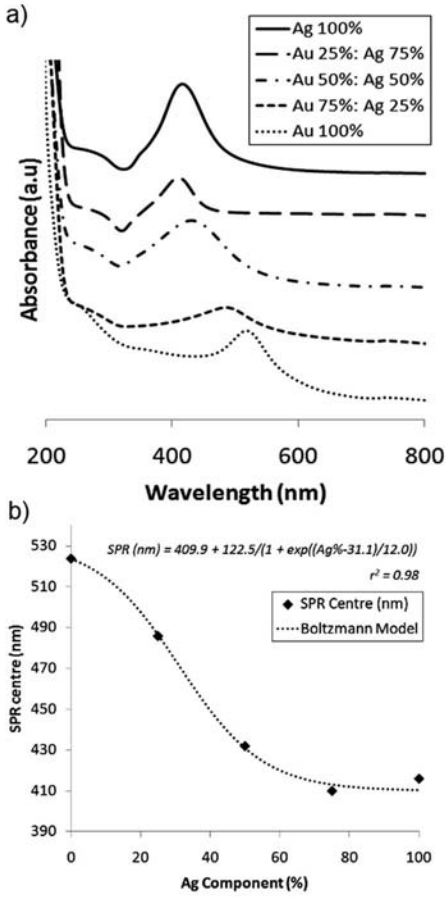

Figure 2. (a) A stacked plot of the normalised UV/Vis absorption spectra and (b) a plot of the resulting SPR centres against the Ag% content for pure Au, Ag and the Au/Ag core-shell nanoparticle colloids that were synthesised by a modified Turkevich thermal co-reduction of the auric acid and/or silver nitrate mixtures.

The diffraction data was then fitted to a Le Bail refined model, which showed an increase in the cell parameter a with an increase in the gold content.[77] The broadness of the diffraction peaks, which is inherent for nanoparticulate materials, demonstrated small crystallite size formation. The average crystallite size was quantified by assessment of the widths of the dominant diffraction peak with (111) symmetry.[78] There was no indication of core-shell formation from the XRD patterns. However, the resolution of the acquired pattern was not of sufficient quality in order to distinguish between the separate Ag and Au symmetries. Nonetheless, the trend in the unit cell parameter a indicated good incorporation of the preformed metal ratios. A list of the XRD parameters and the average crystallite sizes is shown in Table 1. A wide-beam (approximately 10 μm in diameter) EDX analysis of these silica-cast colloids demonstrated compositions that are close to the predetermined Au/Ag ratios. The percentage ratios that were determined by EDX are also shown in Table 1. The samples were cleansed by means of several cycles of centrifugation prior to analysis. This caused any unreacted trisodium citrate reductant, metal ions and reaction biproducts to be decanted from the solution. Therefore, the detection of the presence of any Au and/or Ag metal in these cleansed samples was due to nanoparticle formation. This ultimately showed that the metal ions had completely reacted, regardless of the preformulated Au/Ag ratio, and had been fully incorporated into the colloid as concluded from the good EDX (wide-beam) match and the absence of any Au and Ag in the centrifuge washings.

The size and shape of the nanoparticles in the pure Au (Au 100%), pure Ag (Ag 100%) and the 50:50 Au:Ag mix (Au 50%: Ag 50%) were assessed by HRTEM. The lower magnification sample images for Au 100%, Ag 100% and

Table 1. The UV/Vis spectroscopic SPR centres [nm], the EDX-determined Au content [%], the XRD-derived unit cell parameters and the crystallite Scherrer width [nm], the HRTEM-determined particle diameters [nm], the maximum absorbance increases and the changes in the extinction coefficient, ε, [$M^{-1}cm^{-1}$] from the MB titrations for the optimum ratios for the pure Au, Ag and Ag-Au nanoparticle colloids that were synthesised in this study.

Method	EDX (wide-beam)	XRD		HRTEM	UV/Vis spectroscopy			
Sample	Au component [%]	Unit cell [Å]	Average crystallite size [nm]	Particle diameter [nm]	SPR centre [nm]	Maximum increase in MB absorbance MB:metal	Δ abs.	Δ ε	% ε ↑
Ag 100%	0 ± 0	4.068(1)	13	31.4 ± 12.7	416	0.0144	0.54	1.54×10^5	216
Au 25%:Ag 75%	27.3 ± 1.1	4.072(1)	15	–	410	0.0199	0.49	1.53×10^5	213
Au 50%:Ag 50%	51.4 ± 3.9	4.078(1)	10	46.2 ± 11.7	432	0.0146	0.47	1.34×10^5	187
Au 75%:Ag 25%	72.3 ± 5.3	4.079(1)	13	–	486	0.0126	0.47	1.43×10^5	200
Au 100%	100 ± 0	4.083(1)	13	22.7 ± 3.0	521	0.0090	0.45	1.64×10^5	229

Au 50%: Ag 50% are shown in parts a–c of Figure 4. The particles that were formed in the solitary metal colloids were primarily spherical and had a narrow distribution of sizes. However, more deformed ellipsoidal shapes were seen in the 50:50 mixture with a larger size distribution. A closer observation of this mixture at higher magnification revealed "egg"-like structures that had dense central cores (approximately 20 nm in diameter) and thinner outer shells; such significant differences in TEM image contrast had previously been used to discern core-shell formation alone.[79] Although the lattice fringes could be clearly discerned, HRTEM was unable to differentiate between the core and shell components because of the lack of distinctively different crystallographic features that arose from the almost analogous lattice parameters of the constituent metals.[68] However, the lattice fringes that are present were of the size order that was predicted by Scherrer XRD line broadening (9.5 nm). The particle sizes that were obtained from a series of images were quantified for each of the colloids. For the ellipsoidal particles, the average width about the symmetric horizontal and vertical axes was taken as the diameter. The median particle diameters and the standard deviation errors (nm) are listed in Table 1. The nanoparticles that formed in the pure Au colloid [(22.7 ± 3.0) nm] were significantly smaller and more monodisperse than those that formed in the pure Ag colloid [(31.4 ± 12.7) nm] and the 50:50 mix [(46.2 ± 11.7) nm]. The pure Au colloid consisted of particles that were primarily spherical in shape and had a mean elliptical aspect ratio of 1.08. The majority of the particles in the pure Ag colloid were more ellipsoidal and showed a larger aspect ratio of 1.21. However, the most elliptically natured particles were the Au/Ag core-shells, which displayed deformed ellipsoids that had a mean aspect ratio of 1.37. In order to discern the nature of the Ag-Au composite nanoparticle structures that were observed by HRTEM, a TEM machine that was equipped with a thin-beam EDX probe was used to investigate the 50:50 Au:Ag mix (sample Au 50%: Ag 50%). The EDX spectrum was acquired by focusing an approximately 5 nm wide beam at several positions along the core-shell structures. The ratio of the percentage composition of Ag was determined from the viable counts of the Au M-line and the Ag L-line series. This indicated that the particles were core-shell like (Scheme 1, Type III) in terms of the compositional data, as shown in Figure 5. Although the clarity of the images taken with this instrument was lower, as shown in Figure 4, the "egg"-like shape of the core-shell structure was still clearly discernible.

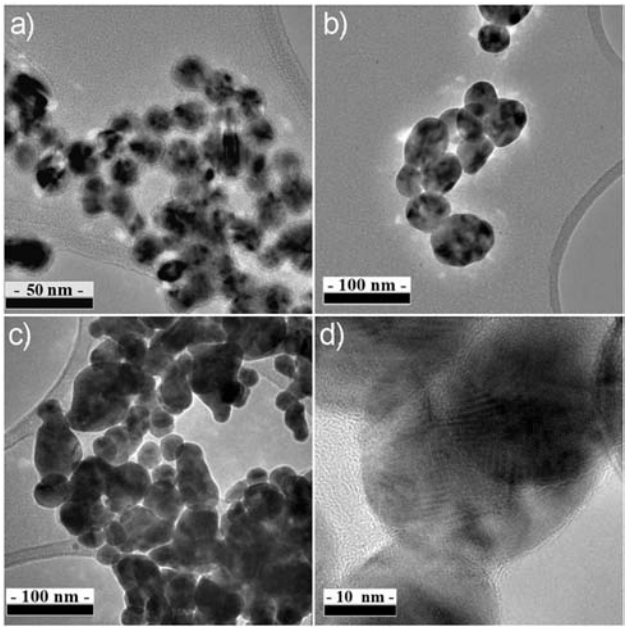

Figure 4. Representative HRTEM images of (a) the pure Au, (b) the pure Ag and (c) and (d) the 50: 50 Au:Ag mix. The particles that were observed in the solitary metal colloids were primarily spherical while deformed ellipsoids and "egg" shapes were seen in the mixture. The colloids were synthesised by a modified Turkevich thermal co-addition of trisodium citrate to the auric acid and silver nitrate mixtures with a predetermined Au/Ag ratio.

A clear increase in the level (Ag counts) and composition (Ag%) of Ag near the centre of the core-shell structure was observed upon moving from position 1 to 2. This was attributed to entry into a more silver-rich core. These two properties decreased nominally from positions 2 to 5, which is reasonable given their proximity to the central core. The subsequent movement to position 6 led to a sharp decrease in the level and composition of Ag. An inverse trend for the Au counts from position 1 to 6 was observed, where a

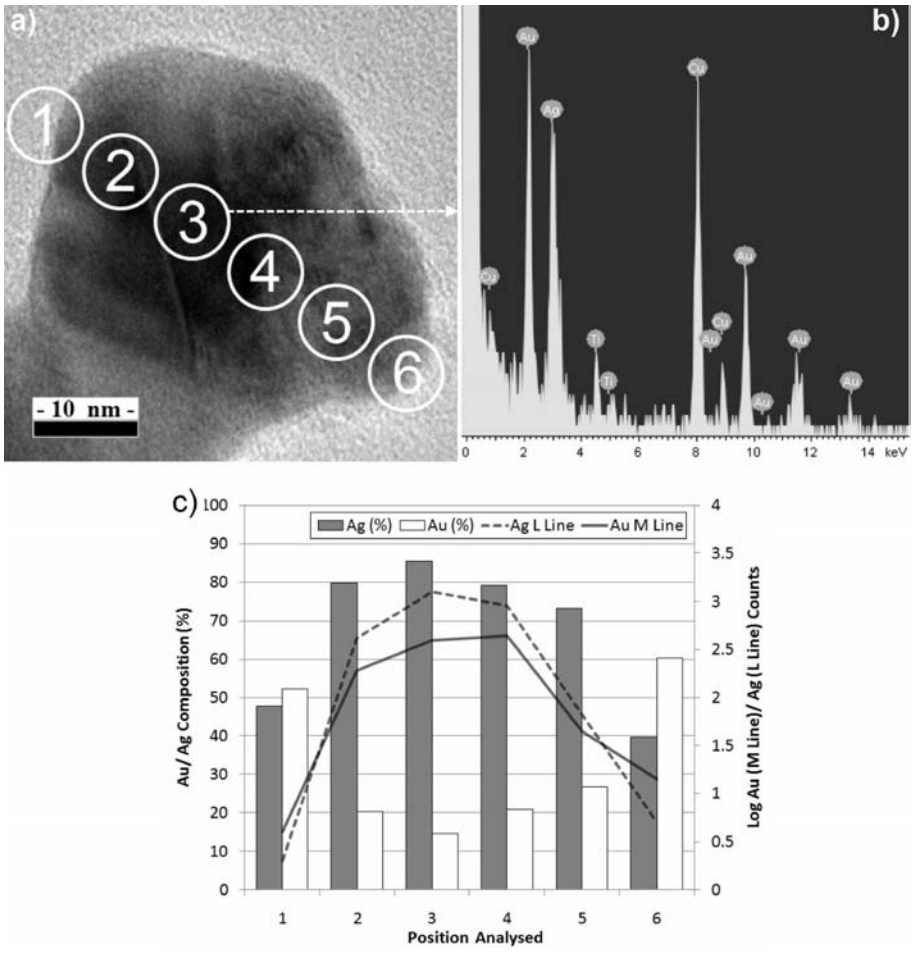

Figure 5. (a) A lower magnification of the TEM image of the Au/Ag core-shell structure with labels that show where thin-beam (approximately 5 nm) EDX analysis was conducted on the Au 50%: Ag 50% colloid, (b) an example of an EDX spectrum at position 3, where Cu and Ti were observed as a result of the holder underneath the sample, and (c) the levels (Au/Ag counts) and the derived Ag composition (Ag%) for each of the analysed positions. These core-shell particles were synthesised by a one-pot thermal co-addition of trisodium citrate to the auric acid and silver nitrate mixtures that had an equivalent Au/Ag ratio.

minimum was observed at position 3 in the central part of the predominantly core-shell particle. The wide-beam EDX analysis results demonstrated an approximately 50:50 incorporation of Ag/Au in the overall bimetallic colloid. This particular nanoparticle was noticeably rich in silver along the axis that was analysed. The fact that the number of counts from the Au M-line and the Ag L-line emissions increased three orders of magnitude from position 1 to the middle positions of the nanoparticle and then decreased three orders of magnitude from the middle position to position 6 indicated that the shape of the nanoparticle was round as it was much thicker at its centre. Four other nanoparticles were assessed in an analogous manner and a dominant Ag core was observed each time. However, both Ag and Au in an approximately equal % ratio were detected in the outer shell coatings. Although the EDX beam was fine-tuned to a diameter of 5 nm, it was impossible to discern how much of the particle was excited upon impact. It could, therefore, not be explicitly discerned whether the core-shell particles formed had a purely Ag core and Au outer shell. However, given the equivalent incorporation of Au and Ag into the particles observed in the wide-beam EDX analysis and the dominant presence of Ag at the core from thin-beam EDX analysis, it was subsequently concluded that the particles consisted of a predominantly Ag core and a Au-rich shell and, hence, that a core-shell Type III structure was formed (Scheme 1).

The Au/Ag core-shell particles have been characterised by using the wide-area EDX beam analysis method (bulk analysis) in conjunction with XPS (surface analysis) and the presence of the core-shell structures have been confirmed.[80] Although this method confirmed the solitary presence of a gold outer layer, the transitional changes from the core outwards were not able to be assessed as they were in this study. The Au/Ag core-shells were also previously assessed by using TEM imaging alone.[79] By modelling the change in the image contrast, the apparent shading of the Ag and Au areas were predicted and applied. However, the level and composition of Au and Ag could not be quantified by this method. Sajanlal et al. used the thin-beam EDX analysis method, which is analogous to that used in this study, to assess the changes in the composition of the Ag/

Au core-shell micron-sized mesoflowers.[81] Although Sajanlal et al. mapped the levels of Au and Ag over a large number of pixels, this technique was not applicable to this study due to the significantly smaller particle sizes (approximately 50 nm) and low counts that result.

XPS was subsequently utilised to investigate the oxidation states of the noble metal ion species in the Au 50%: Ag 50% sample particles. Given the surface sensitivity of XPS, where chemical information from the topmost layers of the sample are acquired (typically several nanometres deep), argon-ion sputtering was utilised to probe the nature of the particles. A thin powder layer of the colloid was cast onto a silica support by continuously dropping solution droplets at the same location between evaporations. Adventitious graphite (1s), at a binding energy of 284.5 eV, was observed in addition to the organic carbon (1s) and carboxylic oxygen (1s) species at binding energies of 289.3 and 530.8 eV, respectively, which were attributed to the citrate surfactant surface layer.[82] No silicon environment from the underlying silica support was seen, which demonstrated that the excitation layer was purely from the colloidal stack. Both the silver and gold environments were observed in high intensity and indicated that the excitation depth was strong enough to probe the cores of the encapsulated core-shell particles (Figures 6, a and b). A solitary Ag^0 environment was observed in the 3d orbital excitation range at binding energies of 368.1 eV ($3d_{5/2}$) and 374.1 eV ($3d_{3/2}$).[83] Two distinct gold environments were observed in the 4f orbital excitation range, with the predominant Au^0 at a binding energy of 84.0 eV ($4f_{7/2}$)[84] and a minor fraction of Au^I was observed at a binding energy of 85.6 eV ($4f_{7/2}$).[85] The ratio of Au^0/Au^I was approximately 3:1. The lone presence of an oxidised gold state correlated with a Ag-Au core-shell model, where the gold shell becomes partially oxidised at the surface.

The sputtering was conducted for two 90 second cycles and with repeat XPS scans in-between. The level of carbon and oxygen was considerably reduced with each cycle as the citrate surfactant layer was removed though sputtering. No additional environments for the noble metals were revealed through sputtering; however, a significant increase in the Ag/Au ratio was observed with each cycle [Figure 6 (c)]. This was attributed to the slow depletion of the Au-rich shell layer with each ion-bombardment, which was supported by evidence from the thin-beam EDX measurements of the Ag-Au core-shell particle nature. Both the bimetallic Ag-Au particles, in addition to the Au-Ag core-shell structures, were formed by a seed-mediated synthesis capped with beta-cyclodextrin surfactant in alkaline solutions by Pande et al.[86] The bimetallic colloids were investigated by XPS, which revealed metallic states for the gold and silver within the core/shell in each case. No surface oxidation was observed. Pande et al. observed both gold and silver environments simultaneously in both of the colloids, which demonstrated that the XPS excitations at the core could penetrate through their encasing shells.

Au/Ag core-shell structures were previously formed by Yang et al. by using a seed-mediated synthesis.[69] The Ag

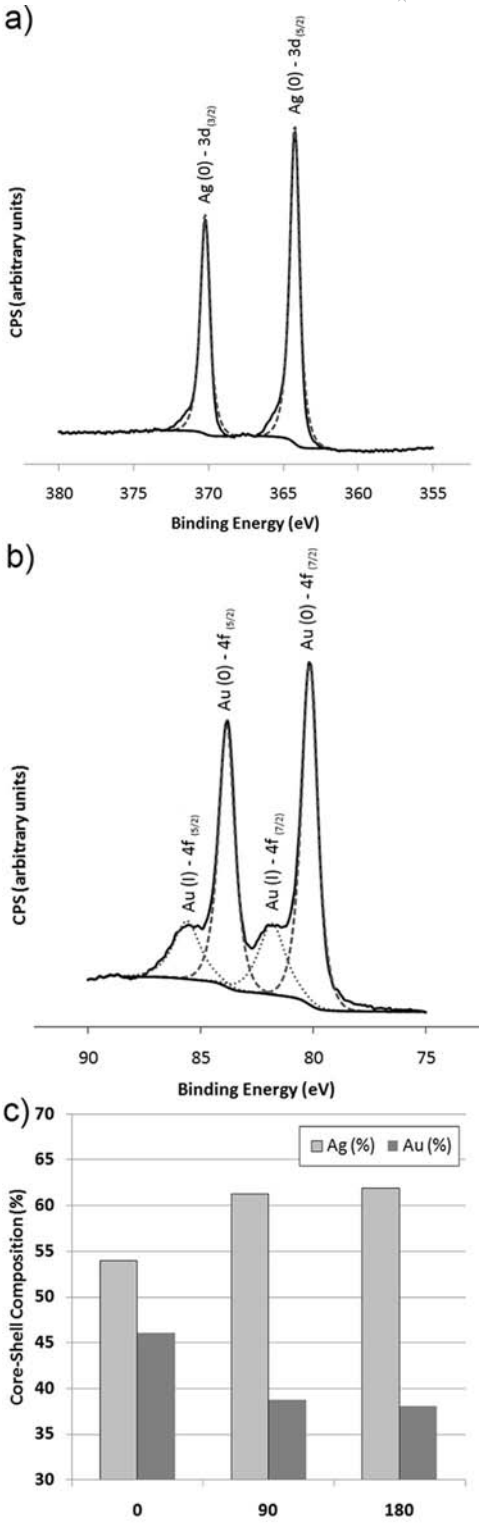

Figure 6. An example of the high-resolution XPS scans of the (a) Ag[3d] and (b) Au[4f] regions before sputtering, (c) shows a plot of the Ag/Au (%) vs. the argon-ion sputtering time (s).

seeds were first formed by heating an aqueous solution of $AgNO_3$ with $NaBH_4$ and a trisodium citrate stabilizer under reflux. These seeds (approximately 9.6 nm in diameter) were then further heated under reflux in a 1:1 ratio with

$HAuCl_4$ and additional stabiliser to form monodisperse core-shells that were less than 9 nm in diameter. In our synthesis, $AgNO_3$ and $HAuCl_4$ salts were similarly reduced by using trisodium citrate, but the $NaBH_4$-induced seed formation step that was utilised by Yang et al. was skipped.[69] This synthesis formed core-shell particles that were contrastingly different in size (46.2 ± 11.7 nm in this study). The formation of considerably smaller particles by Yang et al. was attributed to the use of $NaBH_4$ in the seed formation step, which typically encourages the formation of colloids with comparatively small particles.[80] Similarly, Srnova-Sloufova et al. synthesised Au/Ag core-shell colloids by a two-step seed-mediated aqueous reaction of the preformed Ag seeds [(9 ± 2) nm] with $HAuCl_4$ and hydroxylamine reductant.[79] The resultant nanoparticles were also significantly smaller than those formed in this study, and typically ranged from 8 to 12 nm in size. It was previously shown by Sanchez-Ramirez et al. that the thermal reaction of the $HAuCl_4$ and $AgNO_3$ aqueous mixtures with trisodium citrate at very low metal concentrations can form Au-Ag alloyed colloids.[55] A linear trend in the SPR band position and the Au/Ag content was shown for these alloys, which met the predictions that were made by using a Mie model. In our study, a non-linear variation in the SPR band position was observed. This phenomenon had been observed previously in the literature for other Ag/Au core-shell colloids.[67,68] This study confirmed the presence of Au/Ag core-shell nanoparticles by EDX analysis, which accounted for this discrepancy. Given the predominance of the Ag core, it is reasonable to conclude that a more rapid reaction occurred between $AgNO_3$ and trisodium citrate than between $HAuCl_4$ and trisodium citrate under the imposed experimental conditions. These Ag-rich cores are subsequently encapsulated by the more Au-rich layers from the more slowly reacting $HAuCl_4$.

Methylene Blue Titrations

The nanoparticle colloidal solutions were titrated against methylene blue (MB) solutions of known concentration. A UV/Vis spectrum of aliquots that were taken between the additions enabled the effect on the absorbance of MB at 662 nm (the absorbance maximum of the dye) to be assessed. An example of the MB titration against the 50% Au: 50% Ag core-shell nanoparticles is displayed in Figure 7 (a). A steady increase in the MB profile with the sequential additions was observed. Little deviation from this characteristic profile was observed, even at high MB concentrations. This was indicative of the solitary presence of the monomeric form of MB in solution since the dimer shows a strong absorbance maximum at approximately 620 nm. However, a quenching of the SPR band was observed, which indicated the interaction of the nanoparticles and dye.[89] The magnitude of any increase in the maximum absorbance of MB compared to the dye solutions of an equivalent concentration demonstrated the degree of excitation transfer from the metallic surface to an absorbing dye molecule. The optimum ratio was determined from the derivation of the MB/metal ratio for each of the additions and the subsequent plotting of these ratios against the increase in the MB absorbance [Figure 7 (b)]. The greatest increase in the MB absorption was observed at a MB/metal ratio of 0.0146, which showed that an optimum occurs where approximately 14 MB dye molecules are interacting per 1000 metal atoms. Almost concordantly at this position, the greatest quenching in the SPR band is observed, which suggests a greater excitation transfer from the metal to the dye. All of the colloids demonstrated a positive effect upon the absorbance maximum for the dye, however, by differing degrees (Table 1). At the absorbance maximum, the difference in the extinction coefficient versus the MB dye in water (for the concentration of MB added) was determined by a simple subtraction, which also took into account any original absorbance from the colloid at this wavelength (Table 1). This was then converted into a percentage increase in the extinction coefficient due to the metal–dye in-

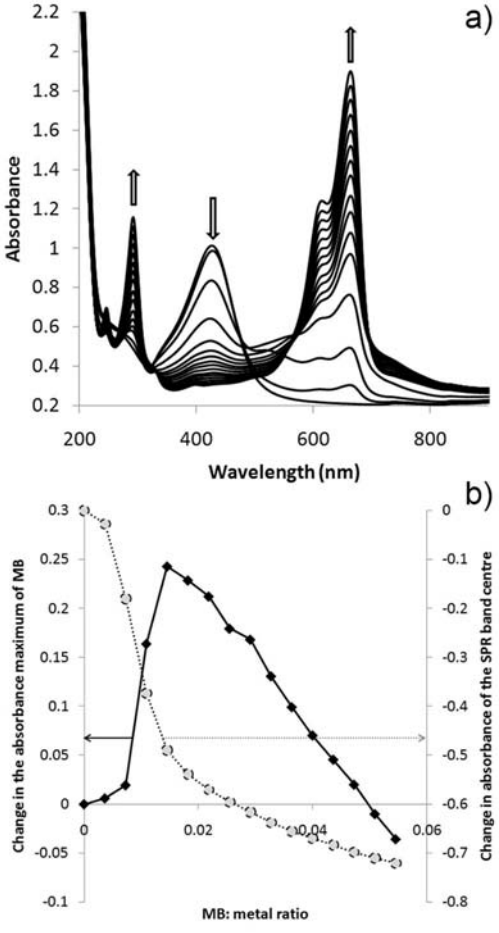

Figure 7. (a) The UV/Vis spectra that were obtained between the additions in the titration of MB against a 20 mL aliquot of the 50% Au: 50% Ag core-shell nanoparticle colloid and (b) the magnitude of the MB increases at 662 nm compared with a standard solution as well as the quenching of the SPR band plotted against the MB/metal ratio. The absorbance maximum occurred at a MB/metal ratio of 0.0146.

teractions relative to the MB dye in the water alone, which could be used for later comparisons with the literature (Table 1).

The maximum increase in the absorbance of the dye (0.54 absorption units) was observed upon titration of the pure silver colloid (Ag 100%). A trend was observed whereby the maximum decreased with the increasing gold content to 0.45 in the pure gold colloid (Au 100%). However, the MB concentration that was present in the solution at this optimum must be taken into account in order to provide a more meaningful quantity, namely, the extinction coefficient increase (ε) of the dye. Given the optimum maximum increase occurred at the lowest MB/metal ratio for the pure Au colloid, the most significant percentage increase of 229% in the extinction coefficient was observed (% ε ↑). This more accurate trend for the effect of the metal–dye interactions showed maxima at the pure Au and Ag ends, while a minimum was observed centrally for the 50:50 mix. This indicated that the interactions with the pure gold yielded the most positive metal–dye interactions. When the average nanoparticle surface area of each colloid and the number of MB molecules that would subsequently surround each particle at the optimum were taken into account, a linear trend was observed with a strong correlation (r^2 = 0.99). This relationship demonstrated the linear dependence of the available surface area per nanoparticle and the number of MB molecules that it could accommodate at the optimum. There are several ways in which a MB dye molecule may interact with a nanoparticle in solution, however, if the two extreme cases are considered, a range of MB coordination shells can be estimated from the titration results. The two cases that we considered are the highest and lowest surface coverage modes, namely, where the MB dye molecule lies completely flat compared to the nanoparticle plane (maximum area is 89.5 Å^2) or points up by means of an interaction of a side amine group to the plane (minimum area is 7.1 Å^2). By making these two assumptions we found an average number of coordination shells that ranged from approximately 0.4 to 5 layers that surround each nanoparticle within the pure gold colloid (Au 100%). Another linear trend was observed (r^2 = 0.97) by comparing each mode of bonding across the tested colloids. In this case a greater particle size yielded a greater number of MB solvation spheres. This result might explain why a lower percentage increase was observed in the extinction coefficient for the comparatively larger Au/Ag core-shell colloid, where a poorer communication resulted between the metal and the dye at the larger average distances. Although the pure Au colloid showed the greatest indication of increased metal–dye interactions, one might attribute it to the larger overall surface area of the sites available for interaction. This meant that a greater amount of surface active sites would be available in the pure Au colloid compared with those in the other colloids that were formed in this study and would therefore better accommodate the dye absorption. For example, when Hyett et al. titrated methylene blue dye against smaller gold nanoparticle colloids [(12 ± 1) nm in diameter], whose concentrations were equivalent to those titrated in this study, an approximately 550% increase in the extinction coefficient was observed, which is more than double the increase observed in this study.[90] However, the total nanoparticle surface area available in 20 mL of a 0.5 mM solution in their gold colloid (170 cm^2) would be almost double the area available in our colloid (90 cm^2). Their maximum extinction coefficient increase also occurred at a dye concentration of 2.2 μM. This was approximately half the level of dye compared with the pure Au titration in this study, where the maximum occurred at a concentration of 4.3 μM. By comparing the titration results across both of the studies, two relationships become clear, namely, that (i) the larger the average nanoparticle size, the greater the distance that is required for the SPR communication and MB to achieve the optimum metal–dye interactions and (ii) the smaller the average nanoparticle size, the lower the MB/metal ratio and the greater the increase in the extinction coefficient that is observed at the optimum (as each metal contributes more effectively and the SPR interaction is spread over a lower number of dye molecules). Within this study, the pure Au and pure Ag colloids showed marginally greater propensities for increasing the extinction coefficient of the MB dye. The near equivalence of the MB dye interactions with the pure Au and Ag colloids were in slight contrast when the height of each of their plasmon bands were solely compared since the pure Ag colloid showed a distinctly larger plasmon absorbance. However, it became clear that the effects are in balance when the number of available surface sites were also taken into account (surface area) since the pure gold colloid consisted of significantly smaller particles and a greater surface area.

The intensely coloured optical response of the gold and silver metallic/bimetallic colloids arises from the dielectric field excitations at the surface of the particles. These photo-induced excitations induce density oscillations, where a collective movement of the electrons gives rise to this intense colour. This process is known as surface plasmon resonance. When the colloid is titrated with cationic dyes such as MB, attraction between the colloid and the dyes leads to the dye absorptions at the surface of the particle. When the titration is done at high dye concentrations, several layers of dye molecules can cover each nanoparticle and, at high enough levels, mass agglomeration ensues. The increase in the MB absorbance has been previously attributed to the transfer of photo-induced plasmons at the nanoparticle surface to the locally surrounding dye molecules.[90] In this study, the core-shell natured colloids showed the lowest extinction coefficient increases when titrated with MB. It was thus assumed that better transfer of the surface plasmons to the local dye molecules occurred in the pure Au and Ag colloids. The detriment of the core-shell like particles was related to two factors, namely, crystallinity and phase barriers. The average crystallite size of the pure Au and Ag colloids decreased from 13 to 10 nm in the 50% Au: 50% Ag sample (Table 1). The less crystalline the sample, the more likely it is that the electron movement will be hindered. In addition, electrons that move across the phase-boundaries

in the core-shell particles would also be hindered. The transfer of the photo-induced dielectric field excitations to the surrounding dye molecules in the core-shell like particles made in this study would therefore be subject to greater recombination effects.

Conclusions

A one-pot modified Turkevich synthesis was used to synthesise a range of colloids from pure Ag, through Au-Ag largely core-shell mixtures to pure Au colloids by the thermal co-addition of trisodium citrate to the auric acid and silver nitrate mixtures. Trends in the SPR band centre indicated the formation of core-shell particles in the Au-Ag mixtures. HRTEM imaging, in conjunction with thin-beam EDX line analysis, confirmed the presence of predominantly Ag cores and Au exteriors. XPS sputtering analysis supported these results with consecutive increases in the level of Ag:Au with increased sputter depth. Two distinct environments were observed in the Au exterior shell. It was thus deduced that a metallic Ag core was covered by a metallic Au shell that was partially oxidised at the surface. Titrations of these colloids against methylene blue dye showed strong positive increases in the extinction coefficient at the absorption maximum. We believe that this is the first time that the efficacy of a range of Ag-Au core-shell like particles to enhance dye colouration has been explored. At the optimum levels of dye addition, a linear relationship between the average nanoparticle size and the number of dye solvation shells that surround it was observed. However, the pure Au and pure Ag particles showed the greatest propensity for the extinction coefficient increase, which may be explained by the better transfer of the surface plasmons to the localised dye molecules.

Experimental Section

All of the reagents were purchased from Sigma–Aldrich UK unless otherwise stated.

Synthesis: All of the glassware was cleaned with aqua regia ($3HCl:1HNO_3$) and rinsed with copious amounts of deionised water prior to use. The aqueous silver nitrate, auric acid and sodium citrate stock solutions were made up in the laboratory. The silver nitrate and auric acid stock solutions consisted of $AgNO_3$ (85 mg) and $HAuCl_4{\cdot}3H_2O$ (170 mg), respectively, which were dissolved up to a volume of 100 mL with distilled water to make up 5 mM solutions. The sodium citrate stock solution consisted of $Na_3C_6H_5O_7{\cdot}2H_2O$ (250 mg) dissolved in distilled water (50 mL, 20 mM). The pure nanoparticle solutions of either gold or silver were synthesised by dissolving the appropriate metal stock solution (2 mL) in distilled water (16 mL) and uniformly heating it in an oil bath with constant stirring. At reflux, the citrate stock (2 mL) was injected into the solution. The solution, with continuous stirring, was heated under reflux for 1 h to ensure complete ripening of the colloid before it was removed from the oil bath. The colour changes of the solution, which were characteristic of gold and silver nanoparticle formation, were observed and went from colourless to lilac to pink to red for the gold synthesis and from colourless to brown for the silver synthesis. Upon cooling the solution to room temperature, the concentrated nanoparticle solution that formed was diluted up to 40 mL total volume (2.5 μM metal content). The gold solutions turned a more pale red and the silver solutions turned a dark yellow upon dilution. The gold-silver alloys with the varying molar ratios were synthesised analogously to the pure nanoparticle solutions by varying the amount of the gold and silver stock solutions that were mixed together (2 mL total volume). The colouration of the eventual solutions varied from pale red, for those colloids that were predominantly Au, to dark yellow, for those colloids that were predominantly Ag solutions.

Methylene Blue Dye Titrations: An aliquot of the synthesised nanoparticle solution (20 mL) was titrated against a stock methylene blue (MB) dye solution, which was made by dissolving a concentrated MB solution (0.46 mL, 1% w/v) (purchased from Alfa Aesar – Johnson Matthey) in distilled water (up to 100 mL). An aliquot (0.25 mL) of the stock solution was added to the test nanoparticle solution and shaken thoroughly. A portion (3 mL) was removed for the UV/Vis spectroscopic assessment and was subsequently returned to the solution. This process was repeated until complete quenching of the surface plasmon resonance (SPR) band was observed.

Analysis: The surface plasmon resonance profiles, as well as the MB titration experiments, were monitored by UV/Vis spectroscopy with a Perkin–Elmer Lambda 25 UV/Vis spectrometer over the 190 to 1000 nm range. Prior to further characterisation, the samples were purified by centrifugation. The solutions were spun at 20,000 rpm (approximately 48,000 × g) for 30 min with a Beckman Coulter Avanti Centrifuge J-26 XP, which caused the nanoparticles to rest at the bottom of the solution. Any biproducts of the solution were removed and replaced with distilled water. The cleansing cycle was repeated twice more. The particle diameters and the core-shell structures were investigated with high resolution transmission electron microscopy with a JEOL JEM-4000 EX HREM and the core-shell compositions were investigated with a JEOL JEM-2010 that was equipped with a thin-beam (diameter ca. 5 nm) EDX probe at Oxford University. The samples were prepared by evaporating the purified solution droplets onto lacey carbon film coated copper grids. A highly concentrated stack of nanoparticles was formed after the continuous evaporation of the purified solution droplets onto the silica substrates on the same spot.

The concentrated stack was subsequently analysed by wide-beam (diameter ≈ 10 μm) energy dispersive X-ray (EDX) analysis, X-ray photoelectron spectroscopy (XPS) that was equipped with a sputter argon-ion gun and glancing angle X-ray diffraction (XRD). The EDX analysis was performed with a JEOL-6301F field emission instrument. The XPS analysis was performed at Cardiff University with a Kratos Axis Ultra-DLD photoelectron spectrometer with monochromatic Al-K_α radiation. The survey and high resolution scans were performed before ion sputtering (90 s) the surface for a total of 3 cycles in order to attain a compositional profile. The survey scans were collected in the range of 0 to 1200 eV (binding energy) at a pass energy of 160 eV. The higher resolution scans were recorded for the principle peaks of Au (4f), Ag (3d), C (1s), O (1s) and Si (2p) at a pass energy of 40 eV. The peaks were modelled with CasaXPS software in order to determine the elemental environment and concentration.[70] The peak positions were adjusted to adventitious carbon (graphite) and the peak areas were adjusted by using sensitivity factors in order to determine the composition.[70] The XRD analysis was conducted with a micro-focus Bruker GADDS powder X-ray diffractometer with a monochromated Cu-$K_{\alpha1}$ (1.5406 Å) source and a CCD area X-ray detector

that was capable of 0.01° resolution in 2θ. The diffraction patterns were compared with the database standards for bulk gold and silver standards and were further analysed by comparison with a Rietveld[70] refined model by using the GSAS and EXPGUI software suite.[71]

Acknowledgments

I. P. P. wishes to thank the Royal Society of Chemistry (RSC) and Wolfsen Trust for a merit award. The Engineering and Physical Sciences Research Council (EPSRC) is thanked for funding and access to the TEM instruments at Oxford Materials under the Materials Equipment Access Scheme grant reference EP/F01919X/1. Cardiff University is thanked for allowing the use of their XPS instrument.

[1] J. F. Sanchez-Ramirez, J. L. Jimenez Perez, A. Cruz Orea, R. Gutierrez Fuentes, A. Bautista-Hernandez, U. Pal, *J. Nanosci. Nanotechnol.* **2006**, *6*, 685.
[2] R. Esparza, G. Rosas, M. Lopez Fuentes, J. F. Sanchez Ramirez, U. Pal, J. A. Ascencio, R. Perez, *Mater. Charact.* **2007**, *58*, 694.
[3] J. L. Rodriguez-Lopez, J. M. Montejano-Carrizales, U. Pal, J. F. Sanchez-Ramirez, H. E. Troiani, D. Garcia, M. Miki-Yoshida, M. Jose-Yacaman, *Phys. Rev. Lett.* **2004**, *92*, 196102.
[4] R. Kubo, *J. Phys. Soc. Jpn.* **1962**, *17*, 975.
[5] M. O. Nutt, K. N. Heck, P. Alvarez, M. S. Wong, *Appl. Catal. B Environ.* **2006**, *69*, 115.
[6] T. Ishii, H. Otsuka, K. Kataoka, Y. Nagasaki, *Langmuir* **2004**, *20*, 561.
[7] A. Sarkar, S. Kapoor, T. Mukherjee, *J. Phys. Chem. B* **2005**, *109*, 7698.
[8] H. Ye, R. M. Crooks, *J. Am. Chem. Soc.* **2007**, *129*, 3627.
[9] P. Hernández-Fernández, S. Rojas, P. Ocón, J. L. Gómez de la Fuente, J. San Fabián, J. Sanza, M. A. Peña, F. J. García-García, P. Terreros, J. L. G. Fierro, *J. Phys. Chem. C* **2007**, *111*, 2913.
[10] A. K. Sharma, B. D. Gupta, *Nanotechnology* **2006**, *17*, 124.
[11] J. H. Liu, A. Q. Wang, Y. S. Chi, H. P. Lin, C. Y. Mou, *J. Phys. Chem. B* **2005**, *109*, 40.
[12] C. Burda, X. Chen, R. Narayanan, M. A. El-Sayed, *Chem. Rev.* **2005**, *105*, 1025.
[13] S. A. Zynio, A. V. Samoylov, E. R. Surovtseva, V. M. Mirsky, Y. M. Shirshov, *Sensors* **2002**, *2*, 62.
[14] M. C. Daniel, D. Astruc, *Chem. Rev.* **2004**, *104*, 293.
[15] R. W. J. Scott, O. M. Wilson, S. K. Oh, E. A. Kenik, R. M. Crooks, *J. Am. Chem. Soc.* **2004**, *126*, 15583.
[16] R. W. J. Scott, A. K. Datye, R. M. Crooks, *J. Am. Chem. Soc.* **2003**, *125*, 3708.
[17] R. Basnayake, Z. Li, Srilakshmi Katar, W. Zhou, H. Rivera, E. S. Smotkin, D. J. Casadonte Jr., C. Korzeniewski, *Langmuir* **2006**, *22*, 10446.
[18] A. M. Molenbroek, S. Haukka, B. S. Clausen, *J. Phys. Chem. B* **1998**, *102*, 10680.
[19] S. A. Lee, K. W. Park, J. H. Choi, B. K. Kwon, Y. E. Sung, *J. Electrochem. Soc.* **2002**, *149*, A1299.
[20] A. Q. Wang, J. H. Liu, S. D. Lin, T. S. Lin, C. Y. Mou, *J. Catal.* **2005**, *233*, 186.
[21] R. Esparza, J. A. Ascencio, G. Rosas, J. F. Sanchez-Ramirez, U. Pal, R. Perez Campos, *J. Nanosci. Nanotechnol.* **2005**, *5*, 641.
[22] R. Ferrando, J. Jellinek, R. L. Johnston, *Chem. Rev.* **2007**, *108*, 845.
[23] L. M. Liz-Marzan, *Langmuir* **2006**, *22*, 32.
[24] P. Mulvaney, *Langmuir* **1996**, *12*, 788.
[25] J. P. Wilcoxon, J. E. Martin, P. Provencio, *J. Chem. Phys.* **2001**, *115*, 998.
[26] M. C. Ferrara, L. Mirenghi, A. Mevoli, L. Tapfer, *Nanotechnology* **2008**, *19*, 365706.
[27] L. Armelao, D. Barreca, G. Bottaro, A. Gasparotto, C. Maccato, C. Maragno, O. I. Lebedev, S. Turner, G. Van Tendeloo, C. Sada, U. L. Strangar, *ChemPhysChem* **2009**, *10*, 3249.
[28] L. Armelao, D. Barreca, G. Bottaro, A. Gasparotto, C. Maccato, C. Maragno, E. Tondello, U. L. Stangar, M. Bergant, D. Mahne, *Nanotechnology* **2007**, *19*, 375709.
[29] A. Ito, H. Masumoto, T. Goto, *Mater. Trans.* **2003**, *44*, 1599.
[30] R. G. Palgrave, I. P. Parkin, *Chem. Mater.* **2007**, *19*, 4639.
[31] R. G. Palgrave, I. P. Parkin, *J. Am. Chem. Soc.* **2006**, *128*, 1587.
[32] R. Binions, C. Piccirillo, R. G. Palgrave, I. P. Parkin, *Chem. Vap. Deposition* **2008**, *14*, 33.
[33] R. G. Palgrave, I. P. Parkin, *Gold Bull.* **2008**, *41*, 66.
[34] G. Walters, I. P. Parkin, *J. Mater. Chem.* **2009**, *19*, 574.
[35] S. Nath, C. Kaittanis, A. Tinkham, J. M. Perez, *Anal. Chem.* **2008**, *80*, 1033.
[36] J. Gil-Tomas, S. Tubby, I. P. Parkin, N. Narband, L. Dekker, S. P. Nair, M. Wilson, C. Street, *J. Mater. Chem.* **2007**, *17*, 3739.
[37] S. Noimark, C. W. Dunnill, M. Wilson, I. P. Parkin, *Chem. Soc. Rev.* **2009**, *38*, 3435.
[38] V. Decrane, A. Rampaul, I. P. Parkin, A. Petrie, M. Wilson, *Curr. Nanosci.* **2009**, *5*, 257.
[39] K. Page, M. Wilson, I. P. Parkin, *J. Mater. Chem.* **2009**, *19*, 3819.
[40] N. Narband, S. Tubby, M. Wilson, I. P. Parkin, J. Gil-Thomas, D. Ready, S. P. Nair, M. Wilson, *Curr. Nanosci.* **2008**, *4*, 409.
[41] S. Perni, C. Piccirillo, J. Pratten, P. Prokopovich, W. Chrzanowski, I. P. Parkin, M. Wilson, *Biomaterials* **2009**, *30*, 89.
[42] P. Ahonen, D. J. Schiffrin, J. Paprotny, K. Kontturi, *Phys. Chem. Chem. Phys.* **2007**, *9*, 651.
[43] C. Yu, H. Nakshatri, J. Irudayaraj, *Nano Lett.* **2007**, *7*, 2300.
[44] M. Li, Y. Lin, C. Wu, H. Liu, *Nucleic Acids Res.* **2005**, *33*, 184.
[45] X. Qian, S. M. Nie, *Chem. Soc. Rev.* **2008**, *37*, 912.
[46] K. Lee, M. A. El-Sayed, *J. Phys. Chem. B* **2006**, *110*, 19220.
[47] W. P. Davey, *Philos. Magn.* **1925**, *50*, 311.
[48] J. Turkevich, P. Stevenson, J. Hillier, *Discuss. Faraday Soc.* **1951**, *11*, 55; E. Jette, F. Foote, *J. Chem. Phys.* **1935**, *3*, 605.
[49] S. Link, Z. L. Wang, M. A. El-Sayed, *J. Phys. Chem. B* **1999**, *103*, 3529.
[50] D. H. Chen, C. J. Chen, *J. Mater. Chem.* **2002**, *12*, 1557.
[51] M. P. Mallin, C. J. Murphy, *Nano Lett.* **2002**, *2*, 1235.
[52] O. M. Wilson, R. W. J. Scott, J. C. Garcia-Martinez, R. M. Crooks, *J. Am. Chem. Soc.* **2005**, *127*, 1015.
[53] B. Rodriguez-Gonzalez, A. Sanchez-Iglesias, M. Giersig, L. M. Liz-Marzan, *J. Chem. Soc. Faraday Trans.* **2004**, *125*, 133.
[54] A. Pal, S. Shah, S. Devi, *Aust. J. Chem.* **2008**, *61*, 66.
[55] J. F. Sanchez-Ramirez, U. Pal, L. Nolasco-Hernandez, J. Mendoza-Álvarez, J. A. Pescador-Rojas, *J. Nanomater.* **2008**, 620412; H. Han, Y. Fang, Z. Li, H. Xu, *Appl. Phys. Lett.* **2008**, *92*, 023116.
[56] S. Devarajan, B. Vimalan, S. Sampath, *J. Colloid Interface Sci.* **2004**, *278*, 126.
[57] Z. Y. Li, J. P. Wilcoxon, F. Yin, Y. Chen, R. E. Palmera, R. L. Johnston, *J. Chem. Soc., Faraday Trans.* **2008**, *138*, 363.
[58] Q. Zhang, J. Y. Lee, J. Yang, C. Boothroyd, J. Zhang, *Nanotechnology* **2007**, *18*, 245605.
[59] Q. Zhang, J. Xie, J. Liang, J. Y. Lee, *Adv. Funct. Mater.* **2009**, *19*, 1387.
[60] Z. Peng, B. Spliethoff, B. Tesche, T. Walther, K. Kleinermanns, *J. Phys. Chem. B* **2006**, *110*, 2549.
[61] Y. Chen, C. Yeh, *Chem. Commun.* **2001**, 371.
[62] B. Karthikeyan, M. Anija, R. Philip, *Appl. Phys. Lett.* **2006**, *88*, 053104.
[63] H. M. Chen, R. S. Liu, L. Y. Jang, J. F. Lee, S. F. Hu, *Chem. Phys. Lett.* **2006**, *421*, 118.
[64] I. Lee, S. W. Han, K. Kim, *Chem. Commun.* **2001**, 1782.
[65] H. Takatani, H. Kago, M. Nakanishi, Y. Kobayashi, F. Hori, R. Oshima, *Rev. Adv. Mater. Sci.* **2003**, *5*, 232.
[66] A. A. Schmidt, R. Anton, *Surf. Sci.* **1995**, *322*, 307.
[67] J. Abid, H. H. Girault, P. F. Brevet, *Chem. Commun.* **2001**, 829.

[68] L. Lu, H. Wang, Y. Zhou, S. Xi, H. Zhang, J. Hu, B. Zhao, *Chem. Commun.* **2002**, 144.
[69] J. Yang, J. Y. Lee, H. P. Too, *Plasmonics* **2006**, *1*, 67.
[70] A. M. Glass, P. F. Liao, J. G. Bergman, D. H. Olson, *Opt. Lett.* **1980**, *5*, 368.
[71] N. Kometani, M. Tsubonishi, T. Fujita, K. Asami, Y. Yonezawa, *Langmuir* **2001**, *17*, 578.
[72] M. A. Noginov, M. Vondrova, S. N. Williams, M. Bahoura, V. I. Gavrilenko, S. M. Black, V. P. Drachev, V. M. Shalaev, A. Sykes, *J. Opt. A: Pure Appl. Opt.* **2005**, S219.
[73] G. Xiao, S. Man, *Chem. Phys. Lett.* **2007**, *447*, 305.
[74] J. W. Chen, J. H. Jiang, X. Gao, J. L. Gong, G. L. Shen, R. Q. Yu, *Colloid Surf. A* **2007**, *294*, 80; W. Haiss, N. T. K. Thanh, J. Aveyard, D. G. Fernig, *Anal. Chem.* **2007**, *79*, 4215.
[75] E. C. Cho, C. Kim, F. Zhou, C. M. Cobley, K. H. Song, J. Chen, Z. Li, L. V. Wang, Y. Xia, *J. Phys. Chem. C Lett.* **2009**, *113*, 9023.
[76] M. A. Uppal, A. Kafizas, T. H. Lim, I. P. Parkin, *New J. Chem.* **2010**, *34*, 1401.
[77] B. H. Toby, *J. Appl. Crystallogr.* **2001**, *34*, 210.
[78] A. L. Patterson, *Phys. Rev.* **1939**, *56*, 978.
[79] I. Srnova-Sloufova, F. Lednicky, A. Gemperle, J. Gemperlova, *Langmuir* **2000**, *16*, 9928.
[80] M. Brust, M. Walker, D. Bethell, D. J. Schiffrin, R. Whyman, *J. Chem. Soc., Chem. Commun.* **1994**, *7*, 801.
[81] P. R. Sajanlal, T. Pradeep, *Langmuir* **2010**, *26*, 8901.
[82] C. D. Wagner, D. A. Zatko, R. H. Raymond, *J. Anal. Chem.* **1980**, *52*, 1445.
[83] G. Schoen, *J. Acta Chem. Scand.* **1973**, *27*, 2623.
[84] J. C. Fuggle, E. Kallne, L. M. Watson, D. J. Fabian, *J. Phys. Rev. B* **1977**, *16*, 750.
[85] H. Kitagawa, N. Kojima, T. Nakajima, *J. Chem. Soc., Dalton Trans.* **1991**, 3121.
[86] S. Pande, S. K. Ghosh, S. Praharaj, S. Panigrahi, S. Basu, S. Jana, A. Pal, T. Tsukuda, T. Pal, *J. Phys. Chem. C* **2007**, *111*, 10806.
[87] G. Jori, C. Fabris, M. Soncin, S. Ferro, O. Coppellotti, D. Dei, L. Fantetti, G. Chiti, G. Roncucci, *Laser Surg. Med.* **2006**, *38*, 468.
[88] G. Bertolini, F. M. Lauro, G. Cortella, M. Merchat, *Biochem. Biophys. Acta* **2000**, *1475*, 169.
[89] K. Bergmann, C. T. O'Konski, *J. Phys. Chem.* **1963**, *67*, 2169.
[90] N. Narband, M. Uppal, C. W. Dunnill, G. Hyett, M. Wilson, I. P. Parkin, *Phys. Chem. Chem. Phys.* **2009**, *11*, 10513.

Received: May 25, 2011
Published Online: September 7, 2011

